Journal of Sound and Vibration (2001) **240**(1), 73–85
doi:10.1006/jsvi.2000.3194, available online at http://www.idealibrary.com on IDEAL®

AN ANALYTICAL AND EXPERIMENTAL INVESTIGATION ON ACTIVE CONTROL OF THE FLEXURAL WAVE TRANSMISSION IN A SIMPLY SUPPORTED RIBBED PLATE

N. J. KESSISSOGLOU

Department of Mechanical Engineering, James Cook University, Townsville QLD 4811, *Australia.*
E-mail: nicole.kessissoglou@jcu.edu.au

(*Received* 9 *June* 1999, *and in final form* 29 *June* 2000)

The feedforward active control of the plate flexural wave transmission along a semi-infinite simply supported ribbed plate has been analytically and experimentally investigated. The ribbed plate was modelled as a continuous system using equations of motion to describe the plate in flexure and the beam in both flexure and torsion. Due to the simply supported and infinite boundary conditions, the structural response is described by a combination of a modal and a travelling wave solution. The primary and secondary sources are modelled as single point forces, with the primary force located on the plate and the secondary control force applied to the reinforcing beam. This force configuration is to demonstrate the feasibility of attenuating the plate response by actively modifying the beam response. Results show that using a single, properly located control actuator and a single error sensor, global attenuation of the transmitted plate vibration through the reinforcing beam is achieved.

1. INTRODUCTION

Active control of the structural vibrations in many plate-type structures is of considerable importance in the maritime and aerospace industries. Vibrations primarily exist in these structures due to mounted machinery or engines, where the vibrating machine can be idealized as a time-harmonic point force excitation on a plate. With significant advances in the technology of materials and electronics used in the components of an active control system, active control will continue to receive considerable attention. Much analytical and experimental work has been carried out to investigate the active control of homogeneous beams [1, 2] and plates [3, 4]. However, the effect of a structural discontinuity such as a reinforcing beam or a structural boundary on the vibrational response of a plate is to alter the nature of the wave propagation in the structure. There has been very little work done on the dynamic response of ribbed plates [5], and only a handful of researchers have examined the active control of the response of ribbed plates [6, 7].

This paper is concerned with applying active control to the reinforcing beam of a ribbed plate to reduce the vibrational response of the transmitted plate waves. The control approach is a steady state feedforward model, where the optimal control force is obtained from the quadratic minimization of a cost function based on the squared plate displacement. Using a single control force located on the beam and a single error sensor, the transmitted vibrational response on a semi-infinite plate at a structural resonance frequency can be significantly attenuated.

0022-460X/01/060073 + 13 $35.00/0

2. ANALYTICAL DEVELOPMENT OF THE BEAM-PLATE MODEL

The ribbed plate consists of a semi-infinite elastic plate symmetrically reinforced by two identical uniform beams of rectangular cross-section, as shown in Figure 1. The beams and plate are simply supported at $y = 0$ and L_y, and the plate is infinite in the x-direction. The beams are located at $x = x_b$. Point force excitation at a location of (x_0, y_0) is used to model the vertically mounted primary shaker used in the experiments, and is described by

$$F(x_0, y_0) = F_0\delta(x - x_0)\delta(y - y_0). \tag{1}$$

Due to the boundary conditions, the structural response is described by both a modal solution in the y-direction, and a travelling wave solution along the x-direction. General solutions for the primary plate response can be obtained for three regions of the plate corresponding to

$$W^P_{1_\mathrm{I}}(x, y) = \sum_{m=1}^{\infty} (A_{1_m}\mathrm{e}^{-\mathrm{j}k_{x_m}x} + B_{1_m}\mathrm{e}^{\mathrm{j}k_{x_m}x} + C_{1_m}\mathrm{e}^{-k_{n_m}x} + D_{1_m}\mathrm{e}^{k_{n_m}x})\sin(k_{y_m}y), \quad x \leqslant x_0 \tag{2}$$

$$W^P_{1_\mathrm{II}}(x, y) = \sum_{m=1}^{\infty} (A_{2_m}\mathrm{e}^{-\mathrm{j}k_{x_m}x} + B_{2_m}\mathrm{e}^{\mathrm{j}k_{x_m}x} + C_{2_m}\mathrm{e}^{-k_{n_m}x} + D_{2_m}\mathrm{e}^{k_{n_m}x})\sin(k_{y_m}y), \quad x_0 \leqslant x \leqslant x_b, \tag{3}$$

$$W^P_2(x, y) = \sum_{m=1}^{\infty} (A_{3_m}\mathrm{e}^{-\mathrm{j}k_{x_m}x} + B_{3_m}\mathrm{e}^{\mathrm{j}k_{x_m}x} + C_{3_m}\mathrm{e}^{-k_{n_m}x} + D_{3_m}\mathrm{e}^{k_{n_m}x})\sin(k_{y_m}y), \quad x \geqslant x_b, \tag{4}$$

where A_{i_m} and B_{i_m} are the coefficients of the propagating waves, and C_{i_m}, D_{i_m} are the coefficients of the near-field decay waves. $k_{y_m} = m\pi/L_y$ is the modal wavenumber along the y-direction, where m is the modenumber. $k_p = (\omega^2\rho_p h/D)^{1/4}$ is the *in vacuo* plate flexural wavenumber, where $D = E_p h^3/12(1 - \nu^2)$ is the flexural rigidity of the plate, and ρ_p, h, E_p and ν are, respectively, the density, thickness, Young's modulus and Poisson's ratio of the plate. $k_{x_m} = \sqrt{k_p^2 - k_{y_m}^2}$ and $k_{n_m} = \sqrt{k_p^2 + k_{y_m}^2}$ are the wavenumbers in the x-direction of the propagating and near-field decay waves, respectively, and are derived from the plate classical equation of motion [4].

The beam–plate system is modelled as a continuous system using the equations of motion to describe the plate in flexure, and the beams in both flexure and torsion. The beam flexural

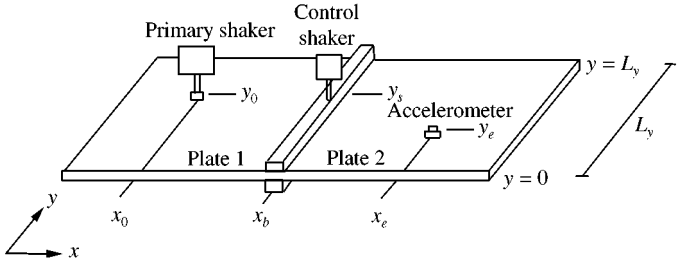

Figure 1. A semi-infinite simply supported ribbed plate showing the locations of the primary and control shakers and the error accelerometer.

and torsional equations of motion are derived as [5]

$$E_b I \frac{\partial^4 u_p}{\partial y^4} + \rho_b A \frac{\partial^2 u_p}{\partial t^2} = \left(Q_{x_2} + \frac{\partial M_{xy_2}}{\partial y} \right)_{x = x_b} - \left(Q_{x_{1\text{II}}} + \frac{\partial M_{xy_{1\text{II}}}}{\partial y} \right)_{x = x_b}, \tag{5}$$

$$GJ \frac{\partial^2 \theta_P}{\partial y^2} - \rho_b I_p \frac{\partial^2 \theta_p}{\partial t^2} = (M_{xx_2})_{x = x_b} - (M_{xx_{1\text{II}}})_{x = x_b}, \tag{6}$$

where $E_b I$ and GJ are the flexural and torsional stiffness of the beam, respectively, and $\rho_b A$, $\rho_b I_p$ are, respectively, the beam mass and polar mass moment of inertia per unit length of beam. Q_x, M_{xx} and M_{xy}, respectively, represent the shear forces, bending moments and twisting moments acting along the unit length of the plates in the y-direction, and are described by the following classical relations:

$$Q_x = -D \frac{\partial}{\partial x} \left(\frac{\partial^2 w}{\partial x^2} + \frac{\partial^2 W}{\partial y^2} \right), \quad M_{xx} = D \left(\frac{\partial^2 W}{\partial x^2} + \nu \frac{\partial^2 W}{\partial y^2} \right), \quad M_{xy} = -D(1 - \nu) \frac{\partial^2 W}{\partial x \partial y}. \tag{7)–(9}$$

In equations (5) and (6), Q_{x_2}, M_{xy_2} and M_{xx_2} are the functions of the primary displacement W_2^p in plate 2 as described by equation (4), and similarly, $Q_{x_{1\text{II}}}$, $M_{xy_{1\text{II}}}$ and $M_{xx_{1\text{II}}}$ are the functions of the primary displacement in the second region in plate 1, $W_{1\text{II}}^p$, as described by equation (3). Due to the boundary conditions, the general solutions for the beam primary flexural and torsional displacement are described by a modal solution.

Twelve unknown coefficients A_{1_m}, $B_{1_m}, \ldots, C_{3_m}$ and D_{3_m} in equations (2)–(4) can be determined from (i) the continuity equations at the driving force location (x_0, y_0); (ii) the continuity equations at the beam–plate boundaries $(x = x_b)$; and (iii) the structural boundary conditions. At the driving force location, there are four coupling equations to describe the continuity of the plate response, corresponding to the continuity of the plate displacement, slope, moment and shear forces

$$W_{1_\text{I}}^p(x_0, y) = W_{1_\text{II}}^p(x_0, y), \quad \frac{\partial W_{1_\text{I}}^p(x_0, y)}{\partial x} = \frac{\partial W_{1_\text{II}}^p(x_0, y)}{\partial x}, \tag{10, 11}$$

$$\frac{\partial^2 W_{1_\text{I}}^p(x_0, y)}{\partial x^2} = \frac{\partial^2 W_{1_\text{II}}^p(x_0, y)}{\partial x^2}, \tag{12}$$

$$\frac{\partial^3 W_{1_\text{I}}^p(x_0, y)}{\partial x^3} - \frac{\partial^3 W_{1_\text{II}}^p(x_0, y)}{\partial x^3} = \frac{2F_0}{L_y D} \sin(k_{y_m} y_0) \sin(k_{y_m} y). \tag{13}$$

Four continuity equations to describe the coupling at the beam–plate boundaries are

$$u_p(y) = W_{1_\text{II}}^p(x_b, y) = W_2^p(x_b, y), \tag{14}$$

$$\theta_p(y) = -\frac{\partial W_{1_\text{II}}^p(x_b, y)}{\partial x} = -\frac{\partial W_2^p(x_b, y)}{\partial x}. \tag{15}$$

The ribbed plate is infinite along the x-direction, and there are no reflected waves from the positive and negative infinities. As a result, the coefficients A_{1_m}, C_{1_m}, B_{3_m} and D_{3_m} are zero. It is possible to solve for the remaining eight unknown coefficients by making use of the eight displacement continuity equations in equations (10)–(15). Using the equations of motion, the continuity equations and the general solutions for the beam and plate displacements,

the following matrix expression is obtained:

$$[\alpha][\mathbf{A}] = [\mathbf{F}], \tag{16}$$

where $[\alpha]$ is an 8×8 matrix, and is given in Appendix A. The coefficient matrix $[\mathbf{A}]$ and the force matrix $[\mathbf{F}]$ are given by

$$[\mathbf{A}] = [B_{1_m}\ D_{1_m}\ A_{2_m}\ C_{2_m}\ D_{2_m}\ A_{3_m}\ C_{3_m}]^{\mathrm{T}}, \tag{17}$$

$$[\mathbf{F}] = \left[0\ 0\ 0\ 0\ 0\ 0\ 0\ \frac{2F_0}{L_y D}\sin(k_{y_m} y_0)\right]^{\mathrm{T}}. \tag{18}$$

Solutions for the unknown coefficients of matrix $[\mathbf{A}]$ are determined by $[\mathbf{A}] = [\alpha]^{-1}[\mathbf{F}]$.

3. ACTIVE CONTROL OF THE PLATE VIBRATION

A point control force of amplitude F_s at a location y_s on the beam generates secondary flexural motion in the beam. The total force acting on the beam consists of two parts: the point force excitation, and the net shear force acting at the boundaries between the beams and plate, which is a result of the backward reaction from the plates acting on either side of the beam [8]. The equation of motion for the secondary flexural waves of the beam excited by a point force is

$$E_b I \frac{\partial^4 u_s}{\partial y^4} + \rho_b A \frac{\partial^2 u_s}{\partial t^2} = F_s \delta(y - y_s) + \left(Q_{x_{s2}} + \frac{\partial M_{xy_{s2}}}{\partial y}\right)_{x = x_b} - \left(Q_{x_{s1}} + \frac{\partial M_{xy_{s1}}}{\partial y}\right)_{x = x_b}, \tag{19}$$

where $Q_{x_{s1}}$ and $M_{xy_{s1}}$ are the functions of the secondary flexural displacement in plate 1 (W_1^s), and similarly, $Q_{x_{s2}}$, $M_{xy_{s2}}$ are the functions of the secondary flexural displacement in plate 2 (W_2^s). General solutions for the plate and beam secondary flexural displacements are

$$W_1^s(x, y) = \sum_{m'=1}^{\infty} (\Phi_{1_{m'}} \mathrm{e}^{\mathrm{j}\sqrt{k_p^2 - k_{y_{m'}}^2}\, x} + \Phi_{2_{m'}} \mathrm{e}^{\sqrt{k_p^2 + k_{y_{m'}}^2}\, x}) \sin(k_{y_{m'}} y), \quad x < x_b, \tag{20}$$

$$W_2^s(x, y) = \sum_{m'=1}^{\infty} (\Phi_{1_{m'}} \mathrm{e}^{-\mathrm{j}\sqrt{k_p^2 - k_{y_{m'}}^2}\, x} + \Phi_{2_{m'}} \mathrm{e}^{-\sqrt{k_p^2 + k_{y_{m'}}^2}\, x}) \sin(k_{y_{m'}} y), \quad x < x_b, \tag{21}$$

$$u_s(y) = \sum_{m'=1}^{\infty} u_{s_{m'}} \sin(k_{y_{m'}} y), \tag{22}$$

where m' is the modenumber of the secondary vibrations, and $k_{y_{m'}} = m'\pi/L_y$ is the modal wavenumber in the y-direction of the secondary waves. From the symmetry of the control force application, the secondary displacements in plates 1 and 2 are the same [9]. $\Phi_{1_{m'}}$ and $\Phi_{2_{m'}}$ are the amplitudes of the plate propagating and near-field decay waves, respectively, and $u_{s_{m'}}$ is the modal amplitude of the beam secondary flexural displacement. The same continuity equations at the beam-plate boundaries exist under secondary excitation of the ribbed plate. However, as the point force control is arranged to only excite the flexural motion in the beam, the secondary torsional displacement in the beam is equal to zero.

Taking the following steps: using equations (7)–(9), (14) and (15) to determine the expressions for the secondary moments and shear forces in terms of the beam secondary flexural displacement; substituting the resultant expressions into the equation of motion described by equation (19); multiplying the resultant equation by an orthogonal mode;

integrating over the length of the beam; and making use of modal orthogonality relationships, results in an expression for the modal amplitude of the beam secondary flexural displacement described by

$$u_{s_{m'}} = \frac{2F_s}{E_b I L_y} H_{f_{m'}} \sin(k_{y_{m'}} y_s), \tag{23}$$

where

$$H_{f_{m'}} = \frac{1}{k_{y_{m'}}^4 - k_B^4 + \dfrac{2\mathrm{j}D}{E_b I}(k_p^4 - k_{y_{m'}}^4)((k_p^2 - k_{y_{m'}}^2)^{-1/2} + \mathrm{j}(k_p^2 + k_{y_{m'}}^2)^{-1/2})} \tag{24}$$

and $k_B = \sqrt{\omega}(\rho_b A/E_b I)^{1/4}$ is the natural flexural wavenumber of the beam. Initial examination of the beam secondary flexural amplitude as a function of frequency shows that the maximum amplitude occurs in the vicinity of resonance frequencies, corresponding to the modal wavenumber in the y-direction being equal to the beam flexural wavenumber ($k_{y_{m'}} = k_B$). It has been previously shown that the maximum plate primary wave transmission by the reinforcing beam occurs at the structural resonance condition occurring when the modal wavenumber of the primary incident wave in the y-direction is equal to the natural flexural wavenumber of the beam [10]. As a result, the beam secondary response is amplified at the structural resonance conditions. At frequencies away from the structural resonances, the secondary response is minimum.

The secondary flexural displacement in plate 1 can be obtained as

$$W_1^s(x, y) = \frac{2F_s}{E_b I L_y} \sum_{m'=1}^{\infty} (\Phi_{1_{m'}} \mathrm{e}^{\mathrm{j}\sqrt{k_p^2 - k_{y_{m'}}^2}\,x} + \Phi_{2_{m'}} \mathrm{e}^{\sqrt{k_p^2 + k_{y_{m'}}^2}\,x}) H_{f_{m'}} \sin(k_{y_{m'}} y_s) \sin(k_{y_{m'}} y), \quad x < x_b, \tag{25}$$

where

$$\Phi_{1_{m'}} = \frac{\sqrt{k_p^2 + k_{y_{m'}}^2}}{\sqrt{k_p^2 + k_{y_{m'}}^2} - \mathrm{j}\sqrt{k_p^2 - k_{y_{m'}}^2}}$$

and

$$\Phi_{2_{m'}} = \frac{-\mathrm{j}\sqrt{k_p^2 - k_{y_{m'}}^2}}{\sqrt{k_p^2 + k_{y_{m'}}^2} - \mathrm{j}\sqrt{k_p^2 - k_{y_{m'}}^2}}$$

represent the coefficients of the secondary propagating and near-field decay waves respectively. Similarly, the secondary flexural displacement in plate 2 is

$$W_2^s(x, y) = \frac{2F_s}{E_b I L_y} \sum_{m'=1}^{\infty} (\Phi_{1_{m'}} \mathrm{e}^{-\mathrm{j}\sqrt{k_p^2 - k_{y_{m'}}^2}\,x} + \Phi_{2_{m'}} \mathrm{e}^{-\sqrt{k_p^2 + k_{y_{m'}}^2}\,x}) H_{f_{m'}} \sin(k_{y_{m'}} y_s) \sin(k_{y_{m'}} y), \quad x > x_b. \tag{26}$$

The plate vibrations are to be minimized at an error sensor location in the far field of plate 2. The total flexural displacement in plate 2 is the superposition of the primary transmitted flexural waves and the secondary flexural waves generated by the point control force, that is

$$W_2^{tot}(x, y) = W_2^p(x, y) + W_2^s(x, y). \tag{27}$$

The primary transmitted flexural waves in the far field of plate 2 can be approximated from equation (4) as

$$W_2^p(x, y) = \sum_{m=1}^{\infty} A_{2_m} \mathrm{e}^{-\mathrm{j}\sqrt{k_p^2 - k_{y_m}^2}\,x} \sin(k_{y_m} y). \tag{28}$$

Similarly, by considering only the propagating secondary waves in the far field of plate 2, equation (26) can be simplified as

$$W_2^s(x, y) = F_s \sum_{m'=1}^{\infty} G_{f_{m'}} \mathrm{e}^{-\mathrm{j}\sqrt{k_p^2 - k_{y_{m'}}^2}\,x} \sin(k_{y_{m'}} y), \tag{29}$$

where

$$G_{f_{m'}} = \frac{2}{E_b I L_y} \Phi_{1_{m'}} H_{f_{m'}} \sin(k_{y_{m'}} y_s). \tag{30}$$

A cost function is developed to minimize the far field flexural energy transmission by means of minimizing the total squared plate displacement at the error sensor. For an error sensor location of (x_e, y_e) in the far field of plate 2, the total power flow at the error sensor location becomes

$$\Pi_f = W_2^{tot}(x_e, y_e)(W_2^{tot}(x_e, y_e))^* \tag{31}$$

By standard methods, the cost function can be expressed as a quadratic function of the control force F_s [2]

$$\Pi_f = F_s A_f F_s^* + B_f F_s^* + F_s B_f^* + C_f, \tag{32}$$

where

$$A_f = \sum_{m'=1}^{\infty} G_{f_{m'}} \mathrm{e}^{-\mathrm{j}\sqrt{k_p^2 - k_{y_{m'}}^2}\,x_e} \sin(k_{y_{m'}} y_e) \left(\sum_{m'=1}^{\infty} G_{f_{m'}} \mathrm{e}^{-\mathrm{j}\sqrt{k_p^2 - k_{y_{m'}}^2}\,x_e} \sin(k_{y_{m'}} y_e) \right)^*, \tag{33}$$

$$B_f = \sum_{m=1}^{\infty} A_{3_m} \mathrm{e}^{-\mathrm{j}\sqrt{k_p^2 - k_{y_m}^2}\,x_e} \sin(k_{y_m} y_e) \left(\sum_{m'=1}^{\infty} G_{f_{m'}} \mathrm{e}^{-\mathrm{j}\sqrt{k_p^2 - k_{y_{m'}}^2}\,x_e} \sin(k_{y_{m'}} y_e) \right)^*, \tag{34}$$

$$C_f = W_2^p(x_e, y_e)(W_2^p(x_e, y_e))^*. \tag{35}$$

Using the orthogonality relationship of the vibrational modes shows that the only non-trivial solution for equation (34) occurs when $m' = m$, and yields

$$B_f = \sum_{m=1}^{\infty} A_{3_m} \mathrm{e}^{-\mathrm{j}\sqrt{k_p^2 - k_{y_m}^2}\,x_e} \sin(k_{y_m} y_e) \left(\sum_{m=1}^{\infty} G_{f_m} \mathrm{e}^{-\mathrm{j}\sqrt{k_p^2 - k_{y_m}^2}\,x_e} \sin(k_{y_m} y_e) \right)^*. \tag{36}$$

Using standard methods, the optimal control force is obtained by differentiating the cost function with respect to the real and imaginary components of the control force, where the optimal force corresponds to both derivatives when they are zero [2]. The optimal control force resulting in the minimum averaged squared plate displacement is obtained as

$$F_s|_{opt} = -\frac{B_f}{A_f}, \tag{37}$$

and the corresponding minimum flexural energy transmission at the error sensor location is

$$\Pi_f|_{min} = C_f - \frac{B_f^* B_f}{A_f}. \tag{38}$$

4. EXPERIMENTAL ARRANGEMENT

4.1. EXPERIMENTAL SET-UP

The experimental rig consists of an aluminium test panel of dimensions 2·4 m × 0·5 m, with a thickness of 1·6 mm. The boundaries of the plate were constructed to simulate the simply supported conditions on two parallel sides of the plate, and infinite conditions on the other two ends. The simply supported boundary conditions of the panel were implemented by using strips of 0·9 mm thick aluminium cut into Z-sections. The upper flanges of the Z-sections were attached to the edges of the panel by small screws at regular intervals. The lower edge of the Z-section was clamped between the concrete blocks. This construction has been previously shown to give a good approximation of a simply supported boundary condition, as the aluminium strips are stiff for in-plane motion but flexible for rotation [10]. To simulate the infinite boundary conditions on the other two edges of the test plate, each panel end was mounted in identical, pyramid-shaded wooden boxes filled with sand. This configuration resulted in the plate flexural waves travelling through the sand boxes to be gradually absorbed by the sand, resulting in no reflected waves from the plate edges. Hence, the sand boxes served to make the plate appear infinite in those directions. A length of 0·6 m of the test plate was placed in the boxes at each end. This gave sufficient length at low frequencies, such that the sand absorbed the structural vibrations with little reflection from the panel edges. The test plate for the experiments had a length of 1·2 m, which was sufficient for the observation of both local and global attenuation.

The solid aluminium beams of length 0·5 m and rectangular cross-section of 10 mm × 10 mm were symmetrically bonded to the surface of the plate using double-sided tape, and were also screwed in three locations. The input disturbance shaker was mounted vertically over the plate, in order to model the primary point force excitation. An impedance head was placed between the electrodynamic shaker and plate in order to measure the acceleration at the driving force location. A mini shaker was used as a control shaker, and was mounted vertically over the beam. Figure 1 is a schematic showing the locations of the primary and control shakers, and the accelerometer. The primary shaker is located at (x_0, y_0) from the sand box and simply supported edge in plate 1, the control shaker is located at a location of y_s on the beam, and the accelerometer used to measure the error signal is located at (x_e, y_e) in plate 2. Figure 2 shows a photograph of the experimental set-up, showing the test panel, reinforcing beams, primary and control shakers, and the structural boundaries.

4.2. CONTROL SET-UP

Active control of the structural response at the error sensor location was performed using feedforward control techniques. An adaptive filtered-X least mean-square (LMS) algorithm was used to conduct the control processing, and was implemented from a digital signal processing board. The program code for the controller was supplied by Bao [11]. The LMS control algorithm is described in detail by Elliott *et al.* [12].

A block diagram of the feed forward adaptive controller is shown in Figure 3. The reference signal to the primary shaker was also fed into the controller. The error signal from

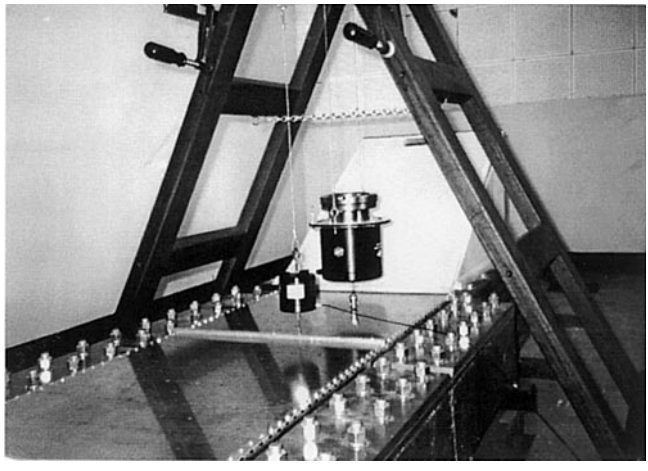

Figure 2. A photograph of the experimental test rig showing the simply supported and infinite boundary conditions, reinforcing beam and mounted primary and control shakers.

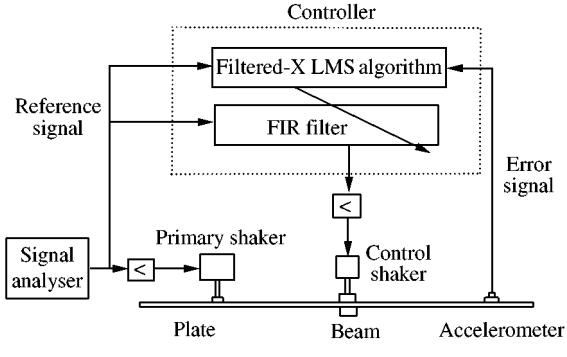

Figure 3. A block diagram of the feedforward adaptive controller.

the accelerometer was also fed into the controller. The controller processed the signals, and produced an optimal signal to drive the control actuator such that the error sensor signal is minimized. The optimized control signal is adjusted by the FIR filter. The weights of the filter are continuously updated using a filtered-X LMS algorithm which minimizes the signal obtained by the error accelerometer. In the experiments, the system identification of the secondary path was modelled by an FIR filter with a filter length of 64 weights, and the sampling frequency was 2000 Hz.

5. RESULTS AND DISCUSSION

5.1. UNCONTROLLED RESULTS

The ribbed plate was constructed entirely of aluminium, where $\rho = 2700\,\mathrm{kg/m^3}$, $E = 6{\cdot}9 \times 10^{10}\,\mathrm{N/m^2}$ and $v = 0{\cdot}33$ are the material parameters. In the analytical modelling, the internal distributed damping in the structure was included in the complex Young's modulus by $\tilde{E}_p = E_p(1 + \mathrm{j}\eta)$, where $\eta = 0{\cdot}001$ is the structural loss factor.

A Hewlett Packard 35665A frequency analyser was used to generate a white-noise signal to excite the plate at the primary shaker location of $(x_0, y_0) = (0{\cdot}2\mathrm{m}, 0.31\mathrm{m})$. The primary

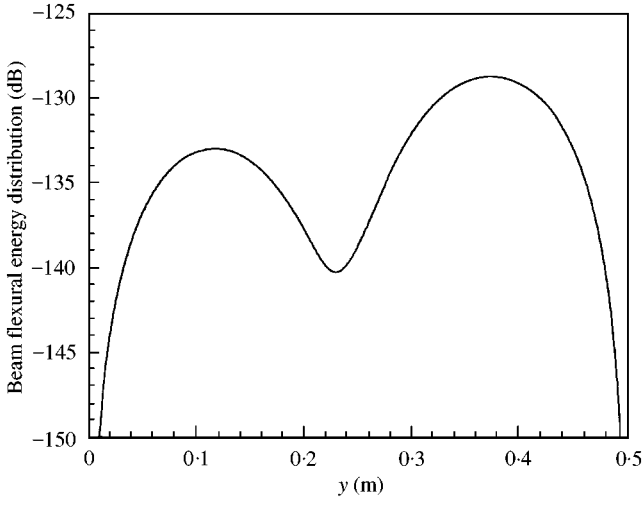

Figure 4. The analytical result of the primary beam response at $f = 312$ Hz.

shaker was located at a position of $y_0 = 0{\cdot}618L_y$ along the width of the plate, resulting in $y_0 = 0{\cdot}31$ m. This corresponds to a structural location which results in the excitation of all the modes. In order to obtain the structural response contributed by all the excited modes, it was important not to place the shaker at the node of the mode. A 2 g Brüel and Kjær accelerometer was used as the error sensor to measure the frequency response at various locations on the plate. The signal from the accelerometer was fed back into the signal analyser via a charge amplifier. Resonance of the beams and plate was observed at a frequency of 312 Hz, which corresponded to the second flexural resonance mode of the beam in the experiments. Figure 4 shows the analytical primary response of the beam at 312 Hz. As shown in the figure, an excitation frequency of 312 Hz corresponds to the second flexural resonance mode of the beam. This frequency was chosen at which to actively attenuate the structural response.

Figure 5 shows both the analytical and experimental uncontrolled responses along the x-direction for $y = 0{\cdot}2$ m and an excitation frequency of 312 Hz. This was experimentally achieved by measuring the structural response at many discrete points along the x-direction starting from the primary shaker location at $x_0 = 0{\cdot}2$ m, and the terminating close to the sand box on plate 2. The reinforcing beams were attached at $x_b = 0{\cdot}5$ m. Figure 5 shows that the response of plate 1 is significantly greater than that of plate 2. At this resonance frequency, the beam already acts as a passive attenuator. Active control at the beam response will further reduce the transmitted vibration.

5.2. CONTROLLED RESULTS

The control shaker was located at $y_s = 0{\cdot}31$ m on the beam in order to excite all the structural modes. In the analytical results, global control of the response in the far field of plate 2 is achieved. Figure 6 shows the primary, secondary and total plate flexural energy distributions along the x-directions, at $y = 0{\cdot}15$ m which corresponds to an anti-node, and at a frequency of 312 Hz. In plate 1 ($x < 0{\cdot}5$ m), there is a slight increase in the total response. However, in plate 2 ($x > 0{\cdot}5$ m), global attenuation of the vibrational response is achieved, with more than 40 dB attenuation at the error sensor location. As expected, the

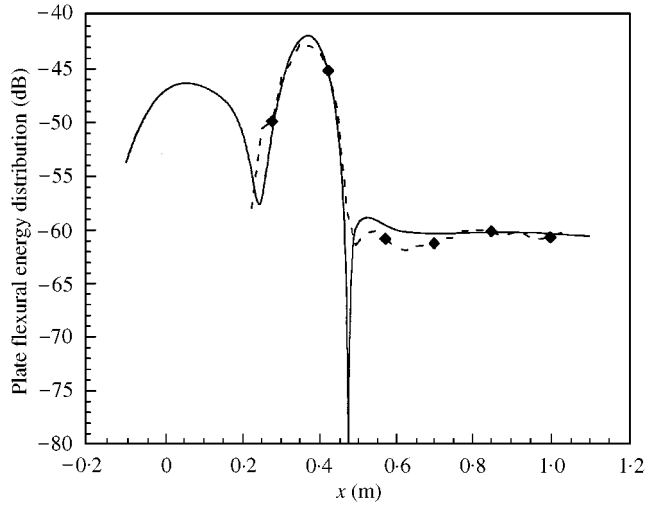

Figure 5. The analytical (——) and experimental (---◆---) uncontrolled responses ($y = 0{\cdot}2$ m, $f = 312$ Hz).

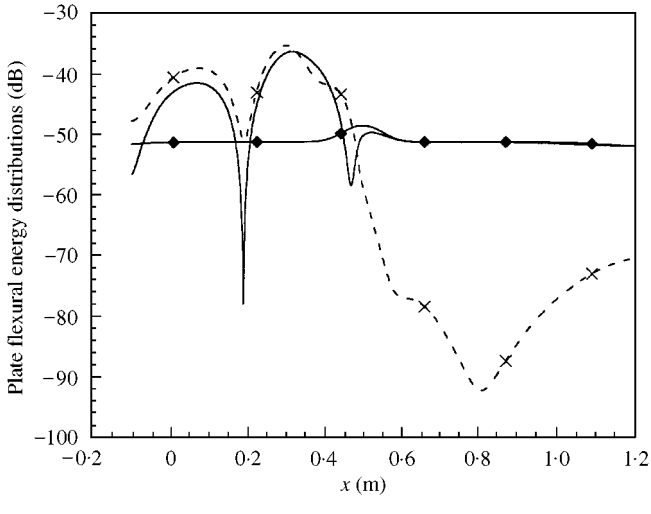

Figure 6. The analytical results showing the primary (——), secondary (—◆—) and controlled (---×---) responses.

secondary response is symmetrical around the beam, and matches the primary response in the far field of plate 2. Figure 7 shows the contour plot of the attenuation level of the ribbed plate obtained analytically for an error sensor location of $(x_e, y_e) = (0{\cdot}8$ m, $0{\cdot}15$ m). This figure shows that the vibrational level in plate 2 has been globally attenuated using a single control actuator applied to the beam and a single error sensor, with dramatic attenuation at the error sensor location. In plate 1, the response has been amplified along the length of the beam. However, in this region, the primary response was dramatically attenuated by the beam (see Figure 5). In the other regions of plate 1, the vibrational response has been both increased by around 5 dB, as well as attenuated by 5 dB at other places.

In the experiments, active control of the structural response at a single error sensor location of $(x_e, y_e) = (0{\cdot}8$m, 0.2m) was performed for an excitation frequency of 312 Hz. Figure 8 shows the uncontrolled and controlled responses along the x-direction for

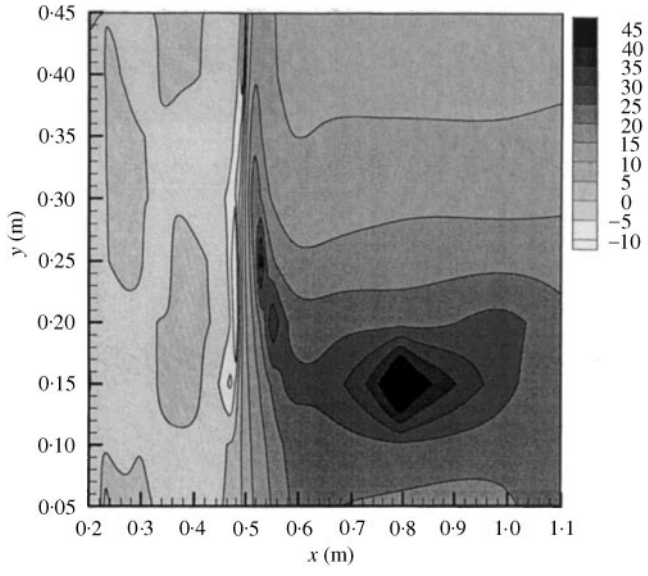

Figure 7. The contour plot of the attenuation level of the ribbed plate obtained analytically.

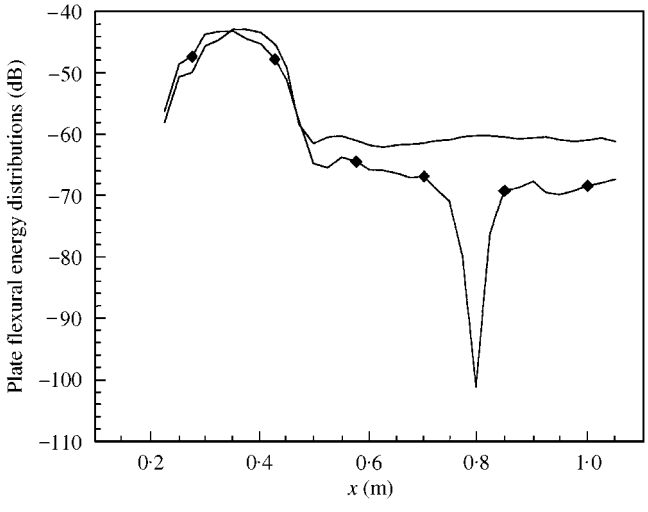

Figure 8. The experimental results showing the uncontrolled (——) and controlled (—◆—) responses.

$y = 0{\cdot}2$ m. Between the primary shaker and the beam ($0{\cdot}2 < x < 0{\cdot}5$), there is very little difference between the uncontrolled and controlled responses. The beam response corresponding to $x = 0{\cdot}5$ m is only slightly attenuated. At the error sensor location ($x = 0{\cdot}8$ m), approximately 40 dB attenuation was achieved. Significant attenuation was also achieved in a region around the error sensor location. Figure 9 shows a contour plot of the attenuation level of the ribbed plate obtained experimentally. In this figure, the vibrational level in plate 2 has been globally attenuated. This result is obtained in addition to the passive attenuation by the beam. At the error sensor location, 40 dB attenuation is observed.

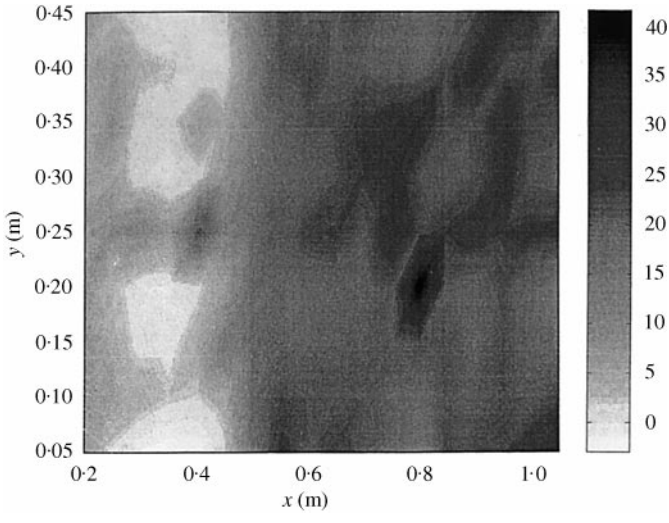

Figure 9. A contour plot of the attenuation level of the ribbed plate obtained experimentally.

6. CONCLUSIONS

In this paper, active attenuation of the plate transmission through reinforcing beams in a ribbed plate was both analytically and experimentally presented. The mathematical modelling was based on a combination of a travelling wave solution and a modal solution. For point force excitation of the ribbed plate, the results obtained from the analytical model were found to agree very well with those obtained experimentally. The control approach consisted of actively modifying the beam response in order to attenuate the plate waves transmitted through the beam. From the uncontrolled results, it was shown that the beam acts as a passive attenuator of the plate transmission through the reinforcing beam. From the control results, the following observations were made:

- using a single control actuator and a single error sensor, global attenuation of the transmitted flexural plate waves through the reinforcing beam was achieved;
- in both the analytical and experimental results, around 40 dB attenuation was observed at the error sensor location; and
- under the control application, very little or no attenuation of the vibration levels in plate 1 was achieved.

REFERENCES

1. J. PAN, C. H. HANSEN and S. D. SNYDER 1992 *Journal of Intelligent Material Systems and Structures* **3**, 39–49. A study of the response of a simply supported beam to excitation by a piezoelectric actuator.
2. J. PAN and C. H. HANSEN 1991 *Journal of the Acoustical Society of America* **89**, 200–209. Active control of total vibratory power flow in a beam: I. Physical system analysis.
3. X. PAN and C. H. HANSEN 1994 *Journal of Intelligent Material Systems and Structures* **5**, 363–370. Piezoelectric crystal vs point force excitation of beams and plates.
4. X. PAN and C. H. HANSEN 1995 *Journal of Sound and Vibration* **184**, 585–610. Active control of vibratory power transmission along a semi-infinite plate.
5. E. E. UNGAR 1961 *Journal of the Acoustical Society of America* **33**, 633–639. Transmission of plate flexural waves through reinforcing beams; dynamic stress concentrations.

6. C. H. HANSEN and A. J. YOUNG 1994 *Proceedings of the 3rd International Congress on Air- and Structure-Borne Sound and Vibration, Montreal, Canada*, 1485–1494. Active control of vibration transmission in a stiffened semi-infinite plate.
7. J. DICKEY and G. MAIDANIK 1991 *Proceedings of the Conference on Recent Advances in Active Control of Sound and Vibration, Virginia Polytechnic Institute and State University, Blacksburg, VA*, 525–533. Active control of response of ribbed panels.
8. G. L. LAMB 1958 *Report No.* 603, *Bolt Beranek and Newman Inc.* Input impedance of a beam coupled to a plate.
9. M. A. HECKL 1961 *Report No.* 774, *Bolt Beranek and Newman Inc.* Compendium of impedance formulas.
10. N. FARAG 1979 *M.Sc. Thesis, Cranfield Institute of Technology*. Comparison of vibration properties of flat panels of various forms of construction.
11. C. BAO 1994 *Ph.D. Thesis, Catholic University of Leuven.* Adaptive algorithms for active noise control and their applications.
12. S. J. ELLIOTT, I. M. STOTHERS and P. A. NELSON 1987 *IEEE Transactions on Acoustics, Speech and Signal Processing* **ASSP-35**, 1423–1434. A multiple error LMS algorithm and its application to the active control of sound and vibration.

APPENDIX A

$$[\alpha] = \begin{bmatrix}
0 & 0 & (1 - \mathrm{j}k_{x_m} H_m \lambda_1)\mathrm{e}^{-\mathrm{j}k_{n_m} x_b} & (1 + \mathrm{j}k_{x_m} H_m \lambda_1))\mathrm{e}^{\mathrm{j}k_{x_m} x_b} \\
0 & 0 & \mathrm{e}^{-\mathrm{j}k_{x_m} x_b} & \mathrm{e}^{\mathrm{j}k_{x_m} x_b} \\
0 & 0 & (\mathrm{j}k_{x_m} - G_m \lambda_3)\mathrm{e}^{-\mathrm{j}k_{x_m} x_b} & (-\mathrm{j}k_{x_m} - G_m \lambda_3)\mathrm{e}^{\mathrm{j}k_{x_m} x_b} \\
0 & 0 & \mathrm{j}k_{x_m}\mathrm{e}^{-\mathrm{j}k_{x_m} x_b} & -\mathrm{j}k_{x_m}\mathrm{e}^{\mathrm{j}k_{x_m} x_b} \\
\mathrm{e}^{\mathrm{j}k_{x_m} x_0} & \mathrm{e}^{k_{n_m} x_0} & -\mathrm{e}^{-\mathrm{j}k_{x_m} x_0} & -\mathrm{e}^{\mathrm{j}k_{x_m} x_0} \\
\mathrm{j}k_{x_m}\mathrm{e}^{\mathrm{j}k_{x_m} x_0} & k_{n_m}\mathrm{e}^{k_{n_m} x_0} & \mathrm{j}k_{x_m}\mathrm{e}^{-\mathrm{j}k_{x_m} x_0} & -\mathrm{j}k_{x_m}\mathrm{e}^{\mathrm{j}k_{x_m} x_0} \\
-k_{x_m}^2\mathrm{e}^{\mathrm{j}k_{x_m} x_0} & k_{n_m}^2\mathrm{e}^{k_{n_m} x_0} & k_{x_m}^2\mathrm{e}^{-\mathrm{j}k_{x_m} x_0} & k_{x_m}^2\mathrm{e}^{\mathrm{j}k_{x_m} x_0} \\
-\mathrm{j}k_{x_m}^3\mathrm{e}^{\mathrm{j}k_{x_m} x_0} & k_{n_m}^3\mathrm{e}^{k_{n_m} x_0} & -\mathrm{j}k_{x_m}^3\mathrm{e}^{-\mathrm{j}k_{x_m} x_0} & \mathrm{j}k_{x_m}^3\mathrm{e}^{\mathrm{j}k_{x_m} x_0}
\end{bmatrix}$$

$$\begin{bmatrix}
(1+k_{n_m} H_m \lambda_2)\mathrm{e}^{-k_{n_m} x_b} & (1-k_{n_m} H_m \lambda_2)\mathrm{e}^{k_{n_m} x_b} & (1+\mathrm{j}k_{x_m} H_m \lambda_1)\mathrm{e}^{-\mathrm{j}k_{x_m} x_b} & (1-k_{n_m} H_m \lambda_2)\mathrm{e}^{-k_{n_m} x_b} \\
\mathrm{e}^{-k_{n_m} x_b} & \mathrm{e}^{k_{n_m} x_b} & \mathrm{e}^{-\mathrm{j}k_{x_m} x_b} & \mathrm{e}^{-k_{n_m} x_b} \\
(k_{n_m} + G_m \lambda_4)\mathrm{e}^{-k_{n_m} x_b} & (-k_{n_m} + G_m \lambda_4)\mathrm{e}^{k_{n_m} x_b} & (\mathrm{j}k_{x_m} + G_m \lambda_3)\mathrm{e}^{-\mathrm{j}k_{x_m} x_b} & (k_{n_m} - G_m \lambda_4)\mathrm{e}^{-k_{n_m} x_b} \\
k_{n_m}\mathrm{e}^{-k_{n_m} x_b} & -k_{n_m}\mathrm{e}^{k_{n_m} x_b} & -\mathrm{j}k_{x_m}\mathrm{e}^{-\mathrm{j}k_{x_m} x_b} & -k_{n_m}\mathrm{e}^{-k_{n_m} x_b} \\
-\mathrm{e}^{-k_{n_m} x_0} & -\mathrm{e}^{k_{n_m} x_0} & 0 & 0 \\
k_{n_m}\mathrm{e}^{-k_{n_m} x_0} & -k_{n_m}\mathrm{e}^{k_{n_m} x_0} & 0 & 0 \\
-k_{n_m}^2\mathrm{e}^{-k_{n_m} x_0} & -k_{n_m}^2\mathrm{e}^{k_{n_m} x_0} & 0 & 0 \\
k_{n_m}^3\mathrm{e}^{-k_{n_m} x_0} & -k_{n_m}^3\mathrm{e}^{k_{n_m} x_0} & 0 & 0
\end{bmatrix},$$

where $\lambda_1 = k_{x_m}^2 + (2 - \nu)k_{y_m}^2$, $\lambda_2 = k_{n_m}^2 - (2 - \nu)k_{y_m}^2$, $\lambda_3 = k_{x_m}^2 + \nu k_{y_m}^2$, $\lambda_4 = k_{n_m}^2 - \nu k_{y_m}^2$,

$$H_m = \frac{2D}{E_b I(k_{y_m}^4 - k_B^4)} \quad \text{and} \quad G_m = \frac{2D}{GJ(k_T^2 - k_{y_m}^2)}.$$